Static-field effects on the nonlinear quantum resonances and the ionization spectrum of a simple bound particle

S. Cocke and L.E. Reichl
Center for Studies in Statistical Mechanics and Complex Systems, The University of Texas at Austin, Austin, Texas 78712
(Received 1 March 1995)

A comparison of nonlinear classical resonances with the nonlinear quantum resonances has been well established for semiclassical systems. However, systems in which tunneling is present are no longer semiclassical and the correspondence between the classical and quantum systems breaks down. We examine nonlinear quantum resonances in a system consisting of a triangular potential well (formed by a static field plus an impenetrable wall) with an attractive δ-function potential well and a weak external time-periodic force. In this system, tunneling is important and nonlinear quantum resonances that have no classical counterpart can occur. In the second part of this paper, we remove the impenetrable wall and consider this system to be a model of a bounded particle subject to a strong external static field and a weak periodic field. The presence of the static field leads to strong enhancement and suppression of the single-photon photodetachment rates for certain frequencies. This effect has been observed experimentally in the photodetachment of H^- ions and predicted by theoretical models. The model present here is particularly useful because the photodetachment spectrum can be obtained analytically and leads to greater insight into more realistic models.

PACS number(s): 32.90.+a, 03.65.Ge, 32.60+i, 42.50.Hz

I. INTRODUCTION

The correspondence between nonlinear resonances in driven conservative classical systems and their quantum analog has been well established for semiclassical systems. This connection between classical and quantum resonances has led to the theory of nonlinear quantum resonance and has been studied in a variety of simple systems [1]. However, few attempts have been made in understanding nonlinear quantum resonances in systems that are not semiclassical. These systems include those in which there is strong tunneling or scattering present. We examine such a system here [2]. In Secs. II and III, we first look at a semiclassical system: a driven triangular potential well formed by combining a linear potential and an impenetrable wall. The driving force is an external time-periodic electric field, such as a laser or microwave. We use the Husimi function to compare the quantum "phase space" with the corresponding classical one.

In Sec. IV, we add an attractive δ function to the model. While the δ function has no effect on the classical system, it leads to tunneling and scattering in the quantum system and the system is no longer semiclassical. We look at the case of a weak external time-periodic field where the resonances are isolated (nonoverlapping). Even though this system may appear to be somewhat artificial, it has an energy spectrum similar to more realistic quantum systems in which tunneling is present. The model should exhibit behavior found in a wide variety of quantum systems, and it is particularly useful in that many calculations can be done analytically or with a minimum of numerical computation. The system may be taken from the nonclassical regime to the semiclassical regime by variation of a single parameter, the strength of the attractive δ potential, thus helping to isolate purely quantal effects.

The attractive δ function itself has proven to be a useful model of a bound particle; the bound state is functionally similar to the ground state of one-dimensional hydrogen [1]. Accordingly, in Sec. V of this paper we shift focus and remove the impenetrable wall, and consider the system as a bound particle subject to a strong static field and a weak periodic field. The single-photon ionization spectrum, which we obtain analytically, exhibits oscillations similar to that observed experimentally in the photodetachment of H^- [3] and predicted in other theoretical models.

II. DRIVEN PARTICLE IN A TRIANGLE POTENTIAL — CLASSICAL SYSTEM

Let us first consider a particle of mass, m, moving in a classical version of a triangular well with no δ function present. If we assume dipole coupling between the particle and the external electric field, we may write the Hamiltonian

$$H=\frac{p^2}{2m}-\epsilon_0 x-\epsilon x\cos(\omega t+\phi_0)+V_L(x), \tag{1}$$

where p is the momentum and x the position of the particle, ϵ_0 is the field strength of the static field, ϵ and ω are the field strength and frequency of the external time-periodic field, and L is the location of the wall. We use atomic units throughout. The potential, $V_L(x)=0$ for $x<L$ and $V_L(x)=\infty$ for $x>L$.

In order to study the nonlinear resonances of the system, it is useful first to rewrite the Hamiltonian, H, in terms of the action-angle variables of the nondriven system,

$$H_0=\frac{p^2}{2m}-\epsilon_0 x+V_L(x)=E_0. \tag{2}$$

The action variable is defined as

$$J=\frac{1}{2\pi}\oint p\,dx=\frac{2\sqrt{2m}}{3\pi\epsilon_0}(E_0+\epsilon_0 L)^{3/2}. \tag{3}$$

Solving for the energy, E_0, we find

$$E_0 = -\epsilon_0 L + \frac{1}{2}\left(\frac{3\pi\epsilon_0}{\sqrt{m}}\right)^{2/3} J^{2/3}. \tag{4}$$

The angle variable can be found from Hamilton's equation,

$$\dot{\theta} \equiv \frac{d\theta}{dt} = \frac{\partial E_0}{\partial J} = \frac{1}{3}\left(\frac{3\pi\epsilon_0}{\sqrt{m}}\right)^{2/3} J^{-1/3}, \tag{5}$$

for the frequency of the orbit. Note that since E_0 is a nonlinear function of J, the frequency, $\dot{\theta}$, is a function of J. The position, x, of the particle in terms of action-angle variables, (J,θ), is

$$x(J,\theta) = -\frac{E_0(J)}{\epsilon_0} + \frac{9\epsilon_0}{2}\left(\frac{\sqrt{m}}{3\pi\epsilon_0}\right)^{4/3} \frac{J^{2/3}\theta^2}{m}, \tag{6}$$

so $x(J,0) = -E_0/\epsilon_0$ is the turning point. It is useful to expand $x(J,\theta)$ in a Fourier series. Then

$$x(J,\theta) = \sum_{n=0}^{\infty} x_n(J)\cos(n\theta), \tag{7}$$

where

$$x_0(J) = \frac{-E_0(J)}{\epsilon_0} + \frac{3\epsilon_0\pi^2}{2m}\left(\frac{\sqrt{m}}{3\pi\epsilon_0}\right)^{4/3} J^{2/3}, \tag{8a}$$

$$x_n(J) = (-1)^n \frac{18\epsilon_0}{mn^2}\left(\frac{\sqrt{m}}{3\pi\epsilon_0}\right)^{4/3} J^{2/3} \quad \text{for } n>0. \tag{8b}$$

The Hamiltonian, Eq. (1), in terms of action-angle variables, is then (with $\phi_0 = 0$)

$$H = E_0(J) - \epsilon \sum_{l=-\infty}^{\infty} x_l(J)\cos(l\theta - \omega t). \tag{9}$$

The external field can now be seen to induce an infinite series of traveling waves into the phase space of the system. Each traveling wave may trap a phase space trajectory and gives rise to a nonlinear resonance [1].

Nonlinear resonance between the external time-periodic driving field and the particle occurs when the field frequency, ω, is a rational fraction of the natural frequency, $\dot{\theta}$, of the particle in the triangular well (this is also the condition that the phase space trajectory becomes trapped in a traveling wave). The *condition for resonance* is then

$$s\omega = l\dot{\theta} = \frac{l}{3}\left(\frac{3\pi\epsilon_0}{\sqrt{m}}\right)^{2/3} J^{-1/3}, \tag{10}$$

where l and s are integers. This resonance is nonlinear because the resonance condition depends on J. The action, J_l, at the center of the lth primary ($s=1$) resonance is $J_l = \pi^2\epsilon_0^2/3m(l/\omega)^3$. The energy at the center of the lth resonance is

$$E_l = -\epsilon_0 L + \frac{\pi^2 l^2 \epsilon_0^2}{2m\omega^2}. \tag{11}$$

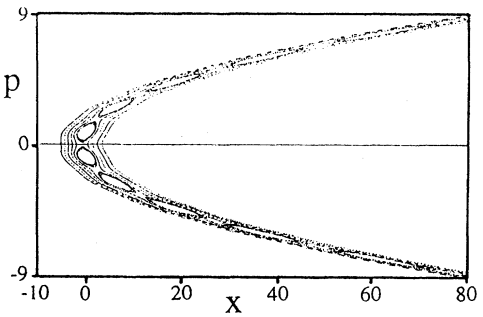

FIG. 1. Classical phase space strobe plot of the system for the parameters $\epsilon = 0.01$, $\omega = 3.59$, and $L = 600$, in the vicinity of the $n = 28$ primary resonance.

In Fig. 1, we show a phase space strobe plot of trajectories of the driven particle in the triangular potential well for the parameters $\epsilon = 0.01$, $\omega = 3.59$, and $L = 600$ (these parameter values were chosen because they allow a sufficient density of states in the quantum calculation described in the next section). The phase space trajectories are obtained by solving Hamilton's equations obtained from the Hamiltonian in Eq. (1). These orbits lie in the vicinity of the $l = 28$ primary resonance. There are a total of 28 "islands" associated with this resonance, of which 10 are shown. The energy of the periodic orbits at the center of the "islands" in Fig. 1 is correctly given by Eq. (11) for $l = 28$.

III. DRIVEN PARTICLE IN A TRIANGLE POTENTIAL — QUANTUM SYSTEM

Next we wish to look at the quantum version of the model. For the unperturbed case ($\epsilon = 0$), the Schrödinger equation for energy eigenstates, $\langle x|n\rangle = \psi_n(x)$ (with energy E_n), becomes

$$-\frac{1}{2m}\frac{\partial^2}{\partial x^2}\psi_n = (E_n + \epsilon_0 x)\psi_n \quad \text{for } x \leq L, \tag{12}$$

where the integer $n = 0,1,\ldots$. The normalized eigenfunctions are given in terms of Airy functions,

$$\psi_n = C_n \mathrm{Ai}\{-[(2m)^{1/3}\epsilon_0^{-2/3}E_n + (2m\epsilon_0)^{1/3}x]\}, \tag{13}$$

where Ai is an Airy function and the normalization constant, C_n, is given by $C_n^{-2} = \mathrm{Ai}'^2\{-[(2m)^{1/3}\epsilon_0^{-2/3}E_n + (2m\epsilon_0)^{1/3}L]\}$ with $\mathrm{Ai}'(x) = d\mathrm{Ai}/dx$.

If we apply a periodic external field ($\epsilon \neq 0$), we may use Floquet theory [1] to study the system. We can obtain the time-evolution matrix, $U_{nn'}$, of the system by integrating the Schrödinger equation,

$$i\frac{\partial}{\partial t}U_{nn'} = E_n U_{nn'} + \sum_{n''} \epsilon\langle n|x|n''\rangle\cos\{\omega t\}U_{n''n'}, \tag{14}$$

subject to the initial condition, $U_{nn'}(t=0) = \delta_{nn'}$. The dipole matrix elements $\langle n|x|n'\rangle$ are given by

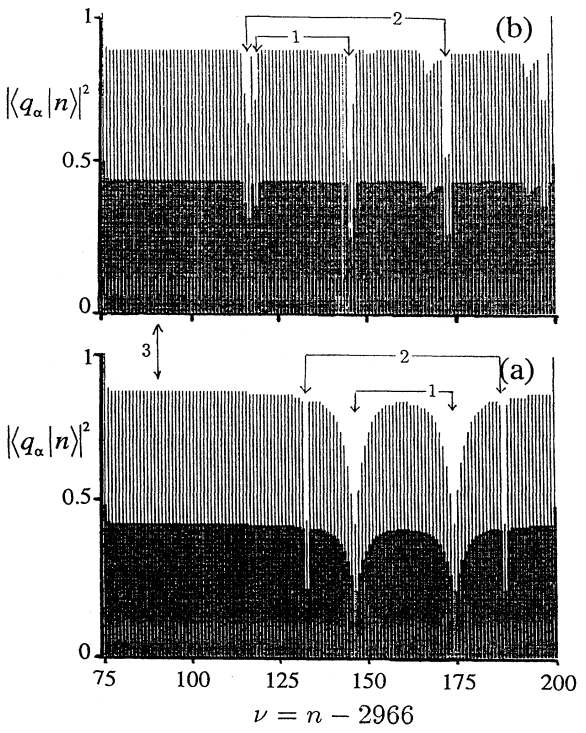

FIG. 2. In each of parts (a) and (b), we plot the overlap probability, $|\langle q_\alpha|n\rangle|^2$ versus n for 125 different Floquet eigenstates (FES), $|q_\alpha\rangle$. In both (a) and (b) $\epsilon=0.01, \omega=3.59$, and $L=600$. A basis set, $|n\rangle$, with n ranging from 2967 to 3167 was used to compute these FES. For all FES except those coupled by resonances, $|\langle q_\alpha|n\rangle|^2\approx 1$. Joined arrows indicate coupled FES for a (1) one-photon resonance, (2) two-photon resonance, and (3) Floquet eigenstate that is nearly equal to an unperturbed eigenstate (up to a phase factor). These were determined by plotting each FES individually. (b) Same system as (a) but with a δ function added ($V=-2.0$), as described in Sec. IV.

$$\langle n|x|n'\rangle=\begin{cases}\dfrac{-\epsilon_0}{m(E_n-E_{n'})^2} & \text{for } n'\neq n\\ \dfrac{2E_n}{3\epsilon_0} & \text{for } n'=n.\end{cases} \tag{15}$$

The energy eigenvalues can be found from the condition that $\psi_n(x=L)=0$. It can easily be shown, using the properties of the roots of the Airy function, that for large n the eigenvalues, E_n, are proportional to $n^{2/3}$. Note that this dependency on n is the same as we get from the classical Hamiltonian [Eq. (4)] when the action is quantized so $J=n\hbar$.

After the time-evolution matrix has been found for one period, we then compute its eigenvectors, $|q_\alpha\rangle$, and eigenvalues q_α. In Fig. 2(a), we plot the overlap probability, $|\langle q_\alpha|n\rangle|^2$, versus n for 125 different eigenvectors, $|q_\alpha\rangle$ (Floquet eigenstates or FES), for the parameters $\epsilon=0.01$, $\omega=3.59$, and $L=600$. The 125 FES shown in the figure were constructed using a basis ranging from $n=2967$ to 3167. For most of the FES, $|\langle n|q_\alpha\rangle|^2$ is a sharply peaked function of n so that $|\langle n|q_\alpha\rangle|^2\approx 1$, and these states remain unaffected by the field. However, at energies, E_n, near -1.4 and 2.17 ($\nu=144$ and 172) there are pairs of FES that strongly couple the unperturbed states, $|n\rangle$ and $|n+28\rangle$ [these are shown by the arrows (1) in the figure and can be seen clearly when we plot the eigenstates separately]. These energies correspond to the one-photon resonance $\omega=E_{n+28}-E_n$. Classically this would be the 28th primary resonance, and its location at the center ($\nu=158$ or $n=3124$) agrees well with the prediction of Eq. (11) for $s=1$, $l=28$, and $J=n$. The analogy between the classical and quantum resonances has been studied in connection with the theory of nonlinear quantum resonances [1]. We can also see another resonance between energies -3.2 and 3.96 ($\nu=130$ and 186 or $n=3096$ and 3152), which are shown by the arrows (2). This is a two-photon resonance corresponding to $2\omega=E_{n+56}-E_n$.

Husimi functions [4] provide an interesting way to compare quantum systems with classical systems. The Husimi function allows us to construct a quantum "phase space" portrait that can be compared to the corresponding classical one. If we introduce the operator $\hat{a}=(\hat{x}+i\hat{p})/\sqrt{2}$, the eigenstate of this operator is a coherent state with a complex eigenvalue $a=(\tilde{x}+i\tilde{p})/\sqrt{2}$, where $\tilde{x},\tilde{p}$ are analogous to the classical phase space variables x,p. The coherent states are minimum uncertainty wave packets centered at (x,p). The coherent states in the position and momentum representations are given by [5]

$$\langle x|a\rangle=\left(\frac{1}{\pi}\right)^{1/4}\exp\left[-\frac{|a|^2}{2}+\frac{a^2}{2}-\left(\frac{x}{\sqrt{2}}-a\right)^2\right]$$

and

$$\langle p|a\rangle=\left(\frac{1}{\pi}\right)^{1/4}\exp\left[-\frac{|a|^2}{2}-\frac{a^2}{2}-\left(\frac{p}{\sqrt{2}}+ia\right)^2\right].$$

The Husimi function for an arbitrary state is given by $W(\tilde{x},\tilde{p})=|\langle\psi|a\rangle|^2$, and gives the probability that a particle lies in the area $d\tilde{x}d\tilde{p}$ centered at $(\tilde{x},\tilde{p})$. The Husimi function can then be written

$$W(\tilde{x},\tilde{p})=\left|\sum_n\int dx\langle\psi|E_n\rangle\langle E_n|x\rangle\langle x|a\rangle\right|^2, \tag{16}$$

where $\langle E_n|x\rangle$ are the eigenfunctions of the unperturbed system and $\langle x|a\rangle$ is given above.

Figure 3 shows plots of Husimi functions for some Floquet eigenstates for the quantum system mentioned above. Compare these plots with the strobe plot for the corresponding classical system given in Fig. 1. The Husimi functions shown in Figs. 3(a) and 3(b) are peaked near the classical fixed points (both stable and unstable). In Fig 3(c) we plot the Husimi function for a Floquet eigenstate which shows a two-photon resonance. There are 56 islands in the two-photon resonance. Only part of the two-photon resonance structure is shown in Fig. 3(c).

IV. TRIANGLE WELL WITH AN ATTRACTIVE δ POTENTIAL

We now construct a nonsemiclassical system by adding an attractive δ potential well to the previous triangular well. The presence of the δ potential will allow for tunneling between the δ well and the triangular well and will introduce interference effects that will alter the eigenspectrum of the system. Let us first consider the case of no external field ($\epsilon=0$). The Hamiltonian becomes (for $\epsilon_0=1$)

$$\hat{H}_0'=\frac{\hat{p}^2}{2m}-\hat{x}+V\delta(\hat{x})+V_L(x), \tag{17}$$

where V is the strength of the δ potential. One can show that in the classical system the δ well has no effect on the system. However, in the quantum case we will have localized and nonlocalized energy eigenstates. [In the limit ($L\to\infty$), the localized states are associated with *virtual levels* for $E>0$ and with a *quasibound state* for $E<0$.] The energy eigenfunctions $\phi_n(x)=\langle x|n\rangle$ of the Hamiltonian H_0' are given by (for $m=1/2$)

$$\phi_n(x)=\begin{cases} N\mathrm{Ai}(\xi), & x\le 0 \\ N\{\mathrm{Ai}(\xi)[1-V\pi\mathrm{Bi}(-E_n)\mathrm{Ai}(-E_n)]+\mathrm{Bi}(\xi)[V\pi\mathrm{Ai}^2(-E_n)]\}, & x>0, \end{cases} \tag{18}$$

where $\xi=-(E_n+x)$ and E_n are energy eigenvalues and

$$N=(\mathrm{Ai}'[-(E_n+L)]\{[1-V\pi\mathrm{Ai}(-E_n)]\mathrm{Bi}(-E_n)\}^2 +\mathrm{Bi}'[-(E_n+L)][V\pi\mathrm{Ai}^2(-E_n)]^2 -2V\mathrm{Ai}'(-E_n)\mathrm{Ai}(-E_n)-V^2\mathrm{Ai}^2(-E_n))^{-1/2} \tag{19}$$

is the normalization integral. The eigenvalues are given by those values of E_n that satisfy the boundary condition $\phi_n(L)=0$. In Fig. 4, we show Husimi plots for typical localized and nonlocalized eigenstates for $V=-2$.

We have compared the difference in energy eigenvalues of the system for $V=0$ and $V=-2$ using 300 states. For $V=0$ the energy spectrum corresponds to the classical case with the quantization condition $J=n\hbar$ ($\hbar=1$ in atomic units). For large negative energies there is essentially no difference due to the presence of the δ well. However there are downward shifts in the $V=-2$ spectrum when the energies

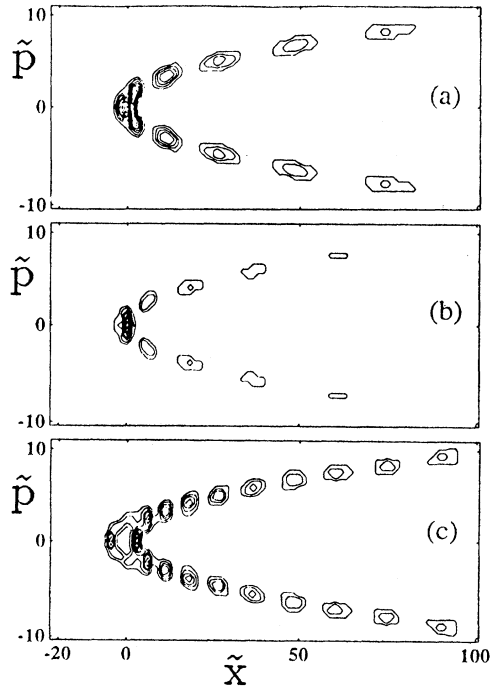

FIG. 3. Husimi function, $W(\tilde{x},\tilde{p})$, contour plots. (a) The one-photon resonance Floquet state for unstable fixed point orbits. (b) The one-photon resonance Floquet state for stable fixed point orbits. (c) The two-photon resonance Floquet state. The Husimi functions are normalized such that the peak value is 1.

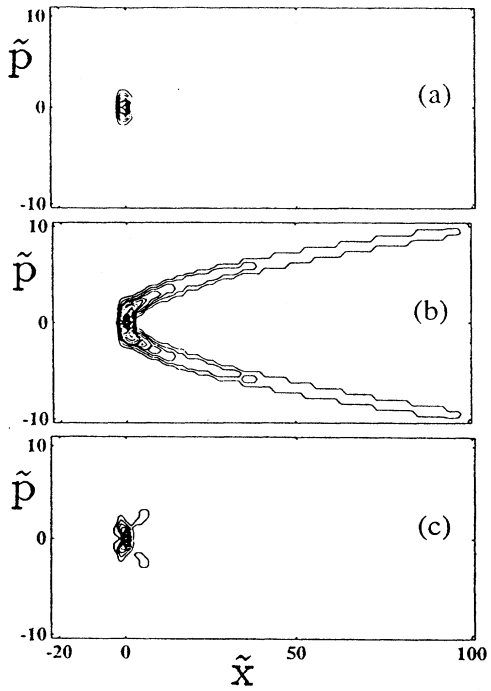

FIG. 4. Husimi function $W(\tilde{x},\tilde{p})$ contour plots of two typical eigenstates. Note that (a) is localized near the δ well, while (b) follows the classical trajectory, and (c) is the Husimi function contour plot of a Floquet state corresponding to a resonance between two localized eigenstates.

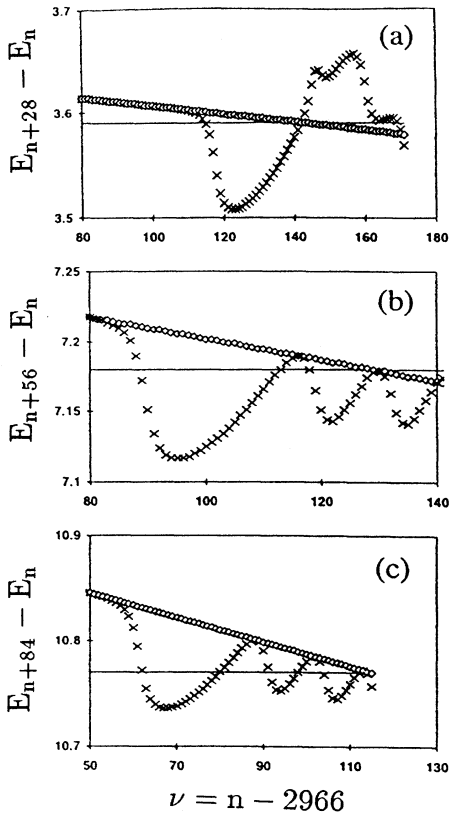

FIG. 5. Graphical solution the (a) one, (b) two, and (c) three-photon resonance condition, using the same basis set as in Fig. 2. The diamond is the energy difference $E_{n+pk}-E_k$ for the $V=0$ case and the crosses for the $V=-2$ case in atomic units. A resonance occurs when a multiple of the photon energy (constant line), $p\omega$, intersects with the energy differences.

are close to the virtual levels. As we shall see below, this has a dramatic effect on the location of the nonlinear quantum resonances. Let us consider the system governed by the Hamiltonian

$$\hat{H}' = \hat{H}_0' + \epsilon\hat{x}\cos(\omega t). \tag{20}$$

In Fig. 2(b), we plot the FES using the same parameters as in Fig. 2(a) but with $V=-2$. States connected by arrows (1) involve a single-photon resonance. States connected by arrows (2) involve a two-photon resonance. The resonance condition for the quantum system is given by $s\omega = E_{n+28s} - E_n$, where s is the number of photons required to make a transition between the $n+28s$th and nth energy levels. In Fig. 5 we show graphically the resonance condition for the one-, two-, and three-photon resonances. The crosses correspond to $V=-2$ and the diamonds correspond to $V=0$. Resonance occurs at the points where the line of crosses or diamonds intersect the horizontal solid line. All of the resonances in Fig. 2 are correctly predicted by the graphical solution in Fig. 5. The oscillations in the energy differences are due to the downward shifts in the energy spectrum

TABLE I. Five of the most localized states and the corresponding poles of the resolvent. Note that the state with negative energy is a remnant of the bound state in the absence of the linear potential.

Localized state	Energy	Real part of pole	Imaginary part
146	−1.20	−1.15	−0.1896
176	2.66	2.66	−0.2042
189	4.33	4.36	−0.2032
200	5.74	5.77	−0.2003
210	7.01	7.01	−0.1973

near the virtual levels. The presence of the δ well creates more, though weaker, resonances. Some resonances are too weak to be observed. The "width" in energy of these resonances depends on the dipole coupling strength between the states.

For the model given in Eq. (17) but with no wall present, Ludviksson [6] has found the resolvent (retarded Green's function) to be

$$G^R(\xi,\xi';z) = G_0^R(\xi,\xi';z) - \frac{G_0^R(\xi,0;z)G_0^R(0,\xi';z)}{V^{-1}+G_0^R(0,0;z)}, \tag{21}$$

where

$$G_0^R(x,x';z) = \begin{cases} -\pi[\mathrm{Bi}(-x'-z)+i\mathrm{Ai}(-x-z)]\mathrm{Ai}(x-z) \\ \quad \text{for } x\leq x' \\ -\pi[\mathrm{Bi}(-x-z)+\mathrm{Ai}(-x'-z)]\mathrm{Ai}(x'-z) \\ \quad \text{for } x>x' \end{cases} \tag{22}$$

The removal of the wall causes the spectrum to be everywhere continuous. If we analytically continue the resolvent into the complex z plane, we pick up poles that give rise to metastable states. The real part of the pole is the energy and the imaginary part is related to the lifetime of the state. There is one pole near the negative real energy axis that corresponds to the semibound state, and an infinite but discrete set of poles near the positive real energy axis that correspond to the virtual levels. For the case with $V=-2$ we can find the poles numerically, and a few are given in Table I. When the wall is present, the eigenstates whose energies are close to the values of the real part of the poles (for no wall) are very localized (cf. Fig. 4). The energies of these eigenstates are also those which locally maximize the normalization integral, Eq. (19).

The existence of virtual levels suggests the interesting possibility of having nonlinear quantum resonances between localized states. In Fig. 4(c) we show a Husimi function of a Floquet state for such a case. Thus, for a sufficiently deep

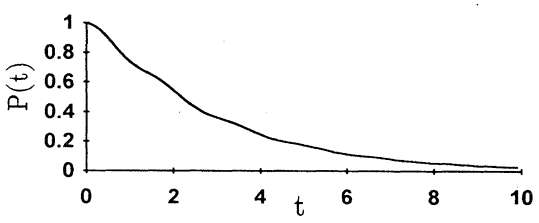

FIG. 6. Survival probability, $P(t)$, as a function of time, t (in atomic units) for the particle initially in the bound state $|\Psi_0\rangle$, for $V=-2.0$.

well (that is, where there is little tunneling), we may have a situation where a particle is coupled to a localized state and fails to reach the wall. We then have Rabi oscillations between the (semi) bound state and one of the localized levels. As the wall is moved away from the atom, these levels become unstable and the oscillations become damped.

V. IONIZATION OF THE "BOUND STATE"

Let us now remove the wall (let $L\rightarrow\infty$). The system consists of a bound particle subject to a strong external static-field and a weak time-periodic field. The spectrum is purely continuous and there are no bound states. First we consider the static-field ionization (no periodic field) of a particle that is initially in the bound state of the attractive δ potential. The wave function of the single bound state is

$$\Psi_0=\sqrt{\frac{|V|}{2}}e^{(V/2)|x|} \tag{23}$$

for $V<0$. When the static field is suddenly turned on, this bound state becomes a superposition of the eigenstates of the combined δ plus linear potential system and decays. In Fig. 6 we show the survival probability

$$P(t)=|\langle\Psi(t)|\Psi_0\rangle|^2, \tag{24}$$

for the case $V=-2$. For practical purposes of numerical computation, we used a large number of eigenstates (more than 100) of the discrete system with $L=600$. The decay of the survival probability is nearly exponential, as expected, but it also has an oscillatory component. The spectral density $\rho(E)=|\Psi_0|E\rangle|^2$ of the initial state in the constant-field basis is shown in Fig. 7. One can distinguish two "Lorentzian" type peaks. The first peak, centered near E_0, gives rise to the overall exponential character of the decay. The states associated with the smaller peak interfere with those of the larger peak and thus produce the oscillatory behavior. These peaks are centered near energies of the virtual levels given in Table I. It is not difficult to understand this oscillatory behavior. The survival amplitude is given by

$$A=\int_{-\infty}^{\infty}e^{-iEt}|\langle\Psi_0|E\rangle|^2dE=\sum_n c_n e^{-iz_nt}, \tag{25}$$

where z_n are the poles of the integrand in Eq. (25). The imaginary part of z_n gives rise to decay. In many systems it

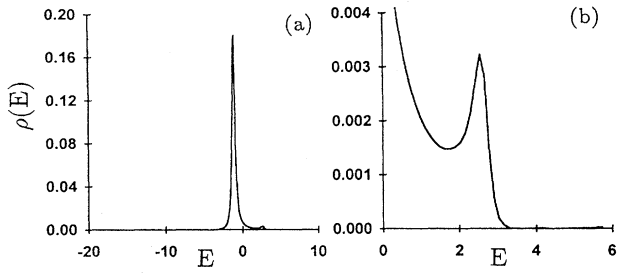

FIG. 7. The spectral density, $\rho(E)=|\langle\Psi_0|E\rangle|^2$, of the initial state in the constant-field basis. (a) The full spectrum. (b) A close-up of the small peak.

is assumed that one pole is dominant ($|\mathrm{Im}z_0|\ll|\mathrm{Im}z_n|$ for all n) and that after a significantly long time, t, all other terms can be neglected. However, if two poles significantly contribute to the survival probability, they will interfere and give rise to oscillations. Note that the survival probability is given by the modulus squared of the amplitude, which results in interference terms. We have computed a few of the poles numerically (cf. Table I) and find the first two significant poles (real part) $z_0=-1.15$ and $z_1=2.66$ to be in agreement with the location of the peaks in Fig. 7. The frequency of the oscillation is easily computed and is found to be $\Omega=\mathrm{Re}(z_1-z_0)$. Figure 8 shows the oscillatory component after the exponential trend has been removed and agrees with the predicted result.

We now consider the photodetachment of a particle subject to a strong external static field. The particle is initially a bound state of the attractive δ potential in the absence of the external static and periodic fields. If the static field is applied, then as we saw above, the state is metastable and eventually decays. (We assume that turn on of the field does not ionize the particle.) The lifetime of this semibound state is $|V|^2\exp(|V|^3)$ [6]. Thus for sufficiently large $|V|$ the particle may be considered bound, and essentially an eigenstate of the static-plus-δ potential. In the presence of a weak external periodic field we may then use perturbation theory to calculate the transition (or photodetachment) rate,

$$W_{0\rightarrow|f|}=2\pi\left(\frac{\varepsilon}{2}\right)^2|\langle\Psi_f|x|\Psi_0\rangle|^2\delta(E_f-E_0-\omega), \tag{26}$$

where Ψ_f are the final continuum states. With the approximation that the lifetime of Ψ_0 being very long, the dipole moment is found to be

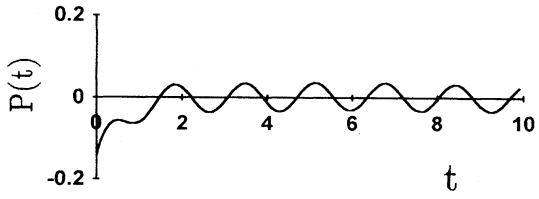

FIG. 8. Survival probability, $P(t)$, with the exponential trend removed.

$$\langle\Psi_f|x|\Psi_0\rangle=\frac{2}{N(E_f-E_0)^2}\{V[\mathrm{Ai}(-E_f)\mathrm{Ai}'(-E_0)+\mathrm{Ai}'(-E_f)\mathrm{Ai}(-E_0)]+V^2\mathrm{Ai}(-E_f)\ \mathrm{Ai}(-E_0)\}, \tag{27}$$

where

$$N=\sqrt{[2V\mathrm{Ai}'(-E_0)\mathrm{Ai}(-E_0)+V^2\mathrm{Ai}^2(-E_0)]\{[1-V\pi\mathrm{Ai}(-E_f)\mathrm{Bi}(-E_f)]^2+V^2\pi^2\mathrm{Ai}^4(-E_f)\}}. \tag{28}$$

When there is no static field present, Geltman [7] has found the dipole moment analytically. In Fig. 9 we plot the transition rates, as a function of frequency, for both the case with a static field and with no static field for $V=-5$. For the case with no static field, the transition rate is smooth and goes to zero for $\omega<E_{\mathrm{ion}}$. However the spectrum is dramatically different when a static field is present. There are values of the frequency of the incident field for which the photodetachment goes to zero, alternating with a series of peak values where the photodetachment is considerably enhanced. These features can be easily understood by examining the expression for the dipole moment, Eq. (27). The peaks occur when N approaches zero. With $\varepsilon=E_f-E_0$ and E_0 fixed, the peaks occur when

$$[1-V\pi\mathrm{Ai}(z_p)\mathrm{Bi}(z_p)]^2+V^2\pi^2\mathrm{Ai}^4(z_p)\rightarrow 0, \tag{29}$$

where $z_p=-(E_0+\varepsilon_p)$. These values of z_p are just the real part of the poles of the resolvent given earlier. Thus photodetachment is very efficient when the bound state is coupled to one of the virtual levels. This is due to the fact that the virtual levels have high probability amplitude near the δ well (between the well and static field barrier). It should be pointed out that the virtual levels are due to the interference between the δ well and the static field barrier, and are not "resonances" of the δ function alone. For a sufficiently deep well, the spacing of the virtual levels are just the spacing of the system where the δ function is replaced by an impenetrable wall, which was described in Secs. II and III. The spacing of the peaks then are proportional to the two thirds power on the incident electric field.

The zeroes in the photodetachment spectrum occur when the numerator in Eq. (27) vanishes. For large V, this happens when $\mathrm{Ai}[-(E_0+\varepsilon)]$ is nearly zero. By examining the expression for N we see that this is nearly true for the peak values as well. This explains why the peaks are very closely spaced to the zeroes. Another way to look at this is as follows: The zeros occur when the continuum wave functions are locally symmetrical about the δ well, whereas the peaks occur at the virtual levels where the probability amplitudes of the continuum wave functions are very high. The locally symmetric states are thus closely spaced to the virtual levels.

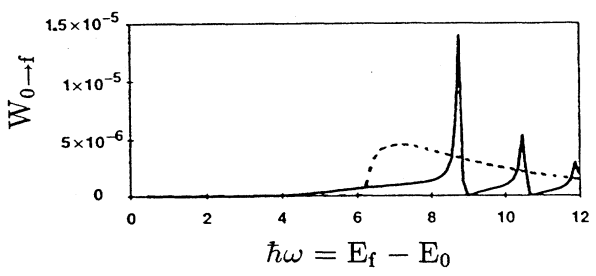

FIG. 9. Plot of the single-photon ionization rates, $W_{0\rightarrow f}$, as a function of photon energy, $\hbar\omega$, for the case of a static field (solid line) versus no static field (dashed line). In both cases $V=-5$.

The photodetachment spectrum presented here is nearly identical to that obtained in a one-dimensional model by Peek [3], but with the δ function replaced by a square well that is shallow enough to support only one bound state. The advantage of the model presented here is that the analytical expression for the dipole moment allows for a more intuitive interpretation of the features of the photodetachment spectrum. For example, the notion of virtual levels and their effect on photodetachment was not mentioned in Ref. [3]. The peaks and zeroes of the photodetachment spectrum are easily calculated numerically for our model. In attempting to gain analytical approximations for the peaks and zeroes in the photodetachment spectrum, Peek and other researchers replace the continuum states with the eigenstates of the static field alone (i.e., without the atomic potential). We may easily do that here. The dipole moment becomes

$$\langle\tilde{\Psi}_f|x|\Psi_0\rangle=\frac{2V\mathrm{Ai}(-E_0)}{(E_0-E_f)^2}\left[\mathrm{Ai}'(-E_f)+\frac{\mathrm{Ai}(-E_f)}{E_0-E_f}\right], \tag{30}$$

where $\tilde{\Psi}_f=\mathrm{Ai}[-(E_f+x)]$ are the eigenstates of the system with static field alone. The peaks are now symmetrical and smoother — not spiked as before. The peaks given by Eq. (30) are at nearly the same energy as in Eq. (27), but the zeros are not. We may interpret this as follows: when the effect of the atomic potential on the continuum is neglected, photodetachment is enhanced when the final continuum states are locally antisymmetric, whereas if we include the effect of the atomic potential the predominant mechanism for the enhancement is the presence of the virtual levels. The locally antisymmetric states $\tilde{\Psi}_f=\tilde{\Psi}_a$ occur at nearly, but not exactly, the same energy as the virtual levels of Ψ_f. If $\Psi_f(x)$ is near a virtual level, then we have a nodal point at $x=0$ and $\Psi_f(0)$ is approximately, but not quite, zero. However, states for which $\Psi_f(0)=0$ are unaffected by the δ potential, i.e., $\tilde{\Psi}_f(x)=\Psi_f(x)$ if $\Psi_f(0)=0$; that is, both the virtual levels Ψ_f and the locally antisymmetric states $\tilde{\Psi}_a$ have a nodal point near $x=0$ for $E_f\approx E_a$. Thus both continua will lead to peaks at nearly the same energy. However, the locally symmetric states of $\tilde{\Psi}_f$ are at very different energies from that of Ψ_f, thus giving different locations in the minima for the dipole moment.

Oscillations of the type described here have been observed in experiments with the photodetachment of negative hydrogen ions [8] and similar experiments. The oscillations in these experimental data appear to be symmetrical, as we would have in the situation predicated by Eq. (30). Thus the virtual levels in these systems may be negligible. However, in any experiment there will be finite resolution due to the lack of monochromicity of the laser pulse, Doppler shifting, etc. Indeed, a course graining of the photodetachment spectrum given in Fig. 9 would give smoother, symmetrical looking peaks. More analysis is needed to determine if the predicted asymmetry can be observed. Nevertheless, this model illustrates a key idea: that static fields can substantially enhance (or reduce) photodetachment rates for a select range of frequencies of an incident electric field.

ACKNOWLEDGMENTS

We wish to thank the Robert A. Welch Foundation, Grant No. F-1051, for support of this work. We also wish to thank the University of Texas System Center for High Performance Computing for use of their computer facilities.

[1] L. E. Reichl, *The Transition to Chaos in Classical Conservative Systems: Quantum Manifestations* (Springer-Verlag, New York, 1992).
[2] Steve Cocke, Ph. D. dissertation, University of Texas at Austin, 1995 (unpublished).
[3] J. M. Peek, Phys. Rev. A **40**, 2393 (1989).
[4] K. Husimi, Proc. Phys. Math. Soc. Jpn. **22**, 264 (1940).
[5] S-J. Chang and K-J. Shi, Phys. Rev. A **34**, 7 (1986).
[6] A. Ludviksson, J. Phys. A. **20**, 4733 (1987).
[7] S. Geltman, J. Phys. B **10**, 831 (1977).
[8] J. E. Stewart *et al.*, Phys. Rev. A **38**, 5628 (1988).